

# Air quality forecasts with observation-based scaling of anthropogenic emissions for urban agglomerations

Adrien Michel Deroubaix<sup>1</sup>, Guy P. Brasseur<sup>1</sup>, Maria de Fatima Andrade<sup>2</sup>, Alejandro Peralta<sup>2</sup>, Phiipp franke<sup>3</sup>, Mario Gavidia-Calderon<sup>2</sup>, Judith Johanna Hoelzemann<sup>4</sup>, Fei Jiang<sup>5</sup>, Inga Labuhn<sup>6</sup>, Laurent MENUT<sup>7</sup>, Nilton Rosário<sup>8</sup>, Guillaume Siour<sup>9</sup>, and rita Yuri Ynoue<sup>2</sup>

<sup>1</sup>Max Planck Institute for Meteorology

<sup>2</sup>Instituto de Ciências Ambientais, Químicas e Farmacêuticas da Universidade Federal de São Paulo

<sup>3</sup>Forschungszentrum Jülich GmbH

<sup>4</sup>Universidade Federal do Rio Grande do Norte

<sup>5</sup>International Institute for Earth System Science, Nanjing University

<sup>6</sup>University of Bremen

<sup>7</sup>Laboratoire de Meteorologie Dynamique

<sup>8</sup>Federal University of Sao Paulo

<sup>9</sup>CNRS/Universités Paris Est-Créteil et Paris Diderot, Institut Pierre Simon Laplace

April 19, 2024

## Abstract

Forecasting urban air quality is important for protecting public health, but current model forecasts are often limited by an inaccurate prescription of pollutant emissions from human activities. We developed a new approach that improves air quality forecasts by adjusting emission prescription based on observed concentrations in urban agglomerations for key pollutants such as nitrogen oxides, sulfur dioxide, carbon monoxide, particulate matter, and volatile organic compounds. Applying this new approach to the São Paulo metropolitan area, Brazil, we compared forecasted and observed pollutant concentrations (from 6 February to 17 April 2023). Using adjusted emission significantly improved air quality forecasts for São Paulo, especially for ozone levels after adjusting estimates of volatile organic compound emissions. However, the forecast of particulate matter concentrations remained challenging due to their links with gaseous pollutants. Our study demonstrates the potential of using observed concentrations in urban agglomerations to improve air quality forecasts. Extending this approach to other urban agglomerations can help refine emission estimates and improve regional air quality forecasts, enabling better decision making for health protection.

# Air quality forecasts with observation-based scaling of anthropogenic emissions for urban agglomerations

Adrien Deroubaix<sup>1,2</sup>, Guy P. Brasseur<sup>1,3</sup>, Maria de Fatima Andrade<sup>4</sup>,  
Alejandro Herman Delgado Peralta<sup>4</sup>, Philipp Franke<sup>5</sup>, Mario  
Gavidia-Calderon<sup>4</sup>, Judith J. Hoelzemann<sup>6</sup>, Fei Jiang<sup>7</sup>, Inga Labuhn<sup>8</sup>, Laurent  
Menut<sup>9</sup>, Nilton Rosario<sup>10</sup>, Guillaume Siour<sup>11</sup>, Rita Yuri Ynoue<sup>4</sup>,

<sup>1</sup>Max Planck Institute for Meteorology, Hamburg, Germany

<sup>2</sup>Institute of Environmental Physics, University of Bremen, Bremen, Germany

<sup>3</sup>National Center for Atmospheric Research, Boulder, Colorado, USA

<sup>4</sup>Instituto de Astronomia, Geofísica e Ciências Atmosféricas, University of São Paulo, Brazil

<sup>5</sup>Institute of Energy and Climate Research - Troposphere (IEK-8), Forschungszentrum Jülich GmbH,  
Jülich, Germany

<sup>6</sup>Graduate Program for Climate Sciences, University of Rio Grande do Norte, Brazil, Natal, Brazil

<sup>7</sup>International Institute for Earth System Science, Nanjing University, China

<sup>8</sup>Climate Lab, Institute of Geography, University of Bremen, Bremen, Germany

<sup>9</sup>Laboratoire de Météorologie Dynamique, Ecole Polytechnique, IPSL, Ecole Normale Supérieure,

Université Paris-Saclay, Sorbonne Université, CNRS, Palaiseau, 91128, France

<sup>10</sup>Environmental Sciences Department, Federal University of São Paulo, Diadema, Brazil

<sup>11</sup>Univ Paris Est Creteil, Université Paris Cité, CNRS, LISA, F-94010 Créteil, France

## Key Points:

- Urban air quality forecasts are improved using observation-based scaling of anthropogenic emissions
- Scaling based on observed-to-modeled concentration ratios increases forecast accuracy
- Ozone concentration forecasts are improved by volatile organic compound emission scaling while assuming a NO<sub>x</sub>-saturated chemical regime

---

Corresponding author: Adrien Deroubaix, [Adrien.Deroubaix@mpimet.mpg.de](mailto:Adrien.Deroubaix@mpimet.mpg.de)

**Abstract**

This study presents a novel approach to improve air quality forecasts in urban agglomerations by scaling anthropogenic emissions on the basis of observed and modeled concentration ratios. Correction factors for emissions of the main primary pollutants, including NO<sub>x</sub>, SO<sub>2</sub>, CO, PM<sub>2.5</sub>, PM<sub>10</sub>, and volatile organic compounds (VOC), are derived by comparing observed and modeled concentrations, assuming that modeled biases are primarily due to inaccuracies in anthropogenic emission inventories. The observation-based scaling approach is applied to the megacity of São Paulo, Brazil, from 6 February to 17 April 2023, demonstrating its effectiveness in refining emission magnitudes and hourly profiles within a short timeframe. We show that the approach significantly improves urban air quality forecasts for NO<sub>x</sub>, SO<sub>2</sub>, and CO after a few weeks. In particular, O<sub>3</sub> concentrations are improved by correcting for VOC emissions, assuming a NO<sub>x</sub>-saturated chemical regime, which is validated by analysis of the modeled and observed chemical regimes. However, improvements for PM<sub>2.5</sub> and PM<sub>10</sub> are limited by their links with primary trace gases that are precursors of secondary aerosols. Overall, this study demonstrates the potential of this approach to be extended to other urban agglomerations, providing valuable top-down constraints to bottom-up global anthropogenic emission inventories and improving regional air quality forecasts.

**Plain Language Summary**

Forecasting urban air quality is important for protecting public health, but current model forecasts are often limited by an inaccurate prescription of pollutant emissions from human activities. We developed a new approach that improves air quality forecasts by adjusting emission prescription based on observed concentrations in urban agglomerations for key pollutants such as nitrogen oxides, sulfur dioxide, carbon monoxide, particulate matter, and volatile organic compounds. Applying this new approach to the São Paulo metropolitan area, Brazil we compared forecasted and observed pollutant concentrations (from 6 February to 17 April 2023). Using adjusted emission significantly improved air quality forecasts for São Paulo, especially for ozone levels after adjusting estimates of volatile organic compound emissions. However, the forecast of particulate matter concentrations remained challenging due to their links with gaseous pollutants. Our study demonstrates the potential of using observed concentrations in urban agglomerations to improve air quality forecasts. Extending this approach to other urban agglomerations can help refine emission estimates and improve regional air quality forecasts, enabling better decision making for health protection.

**1 Introduction**

Air quality forecasting in urban agglomerations is complex due to the strong diurnal evolution of pollutant emissions and concentrations in the urban boundary layer (Baklanov et al., 2016). Forecasting air quality is one of the main objectives in developing deterministic air quality chemistry and transport models to provide early warning to the population on serious air quality deterioration, particularly for O<sub>3</sub> and aerosols (Carmichael et al., 2008).

COVID19 has also shown that, under certain circumstances, human habits can change dramatically, leading to sudden changes in pollutant emissions and concentrations. Thanks to platforms that gather data from different air quality monitoring networks (Kosmidis et al., 2018), it becomes possible to analyze the change in atmospheric composition using near-real time observations. Using the OpenAQ data platform, Venter et al. (2020) showed that the decrease in anthropogenic emissions, mainly related to traffic, has led to an overall improvement in air quality, although O<sub>3</sub> concentrations have increased in several major urban agglomeration, for example in Europe (Deroubaix et al., 2021). To

76 accurately reproduce global changes in atmospheric composition with an air quality model  
77 (Gaubert et al., 2021), the model first requirement are updated and accurate global an-  
78 thropogenic inventory as input (Dombia et al., 2021). In addition, the air quality fore-  
79 casting system based on an ensemble of models developed for China (Petersen et al., 2019;  
80 Brasseur et al., 2019) showed that during the COVID19 lockdowns only one model was  
81 able to adapt to the rapid change in emissions and predict O<sub>3</sub> concentrations in agree-  
82 ment with observations. This model uses a method for adjusting anthropogenic emis-  
83 sions.

84 Due to the large uncertainties in emission inventories, observation-based data as-  
85 similation methods have been developed in the last two decades using satellite-based ob-  
86 servations of vertical pollutant profiles and observations from air quality monitoring net-  
87 works, which have greatly contributed to improving the performance of air quality fore-  
88 casts (e.g. Carmichael et al., 2008; Bocquet et al., 2015; Carrassi et al., 2018). However,  
89 the application of these methods to air quality forecasting in urban agglomerations is  
90 limited due to the coarse spatial resolution of satellite data and issues related to the spa-  
91 tial implementation of the monitoring network (Nguyen & Soulhac, 2021). Anthropogenic  
92 emissions in air quality models are generally provided by bottom-up emission invento-  
93 rories calculated by species and sector of activity (Brasseur & Jacob, 2017). The bottom-  
94 up method allows global emissions to be quantified on the basis of current knowledge of  
95 species driving processes that are not directly constrained by observed concentrations.  
96 Consequently, concentrations modeled from a bottom-up emission inventory may not be  
97 consistent with observations, which can be improved by anthropogenic emissions adjust-  
98 ment methods prescribed in the model. Top-down constraints derived from atmospheric  
99 observations are used to optimize emissions by applying correction factors to bottom-  
100 up emissions (Brasseur & Jacob, 2017).

101 The discrepancies between global and local anthropogenic emission inventories are  
102 particularly important for cities, for example in South America (Huneeus et al., 2020)  
103 and especially for vehicular emissions (Ibarra-Espinosa et al., 2020). Nowadays, there  
104 is a growing number of air quality monitoring networks implemented with low-cost sen-  
105 sors. Even if the accuracy of the sensors is discussed (e.g. Kumar et al., 2015; Castell  
106 et al., 2017; Wesseling et al., 2019), their rapid implementation with a large number of  
107 sensors provides satisfactory information to estimate pollutant concentrations averaged  
108 at the scale of an urban agglomeration, especially for those without a monitoring net-  
109 work (e.g. Kumar et al., 2015; Park et al., 2020). These local concentration observations  
110 must serve as top-down constraints on emissions to enable reliable air quality modeling  
111 in urban agglomerations where regional ensemble forecasts are not available.

112 This article presents a study on regional air quality forecasting with a scaling ap-  
113 proach to impose top-down constraints on anthropogenic emissions adapted to urban ag-  
114 glomerations. We explain the emission scaling approach and the improvements expected  
115 for regional air quality forecasting (Section 2). Regional air quality forecasts with the  
116 anthropogenic emission scaling approach are applied to São Paulo for a period of 10 weeks  
117 in the year 2023 (from 6 February to 17 April 2023), which is comparable to the dura-  
118 tion of an observational field campaign (Section 3). The evolution of the statistical per-  
119 formance of the regional forecasts is investigated for the main regulated pollutants, *i.e.*  
120 carbon monoxide (CO), nitrogen dioxide (NO<sub>2</sub>), ozone (O<sub>3</sub>), sulfur dioxide (SO<sub>2</sub>), as well  
121 as PM<sub>2.5</sub> and PM<sub>10</sub> (Section 4). Finally, development perspectives and limitations of the  
122 anthropogenic emission scaling approach are discussed (Section 5).

## 123 2 Air quality forecasts with anthropogenic emissions scaling

124 In this section, we explain the motivation for providing regional air quality fore-  
125 casts for urban agglomerations (Section 2.1), the requirements for the monitoring net-

work (Section 2.2), the observation-based scaling approach of anthropogenic emissions (Section 2.3), and the limitations of the approach (Section 2.4).

## 2.1 Regional forecasts for urban agglomerations

The proposed approach to improve regional air quality forecasting is aimed at urban agglomerations that do not have an operational air quality forecasting system. In urban agglomerations, anthropogenic emission sources are dominant, and modeling errors in the concentration of short-lived primary species are mainly related to anthropogenic emissions, both in terms of magnitude and hourly profiles (e.g. Viaene et al., 2016).

Global inventories of anthropogenic emissions are often provided at a spatial resolution of 10 km (e.g. Huang et al., 2017). When they are used for global forecasts at a coarser resolution than 10 km, their information is degraded. Consequently, regional forecasts at 10 km should outperform global forecasts due to the improved spatial representation of primary pollutant emissions. Nevertheless, to provide regional forecasts with a timescale much shorter than one day, efficiency is a major constraint, requiring small horizontal modeling domains focused on urban agglomerations and configurations with chemical and aerosol models that require low computational resources. The proposed approach is dedicated to large urban agglomerations, such as megacities, where anthropogenic emissions can be assumed to be dominant.

## 2.2 Spatial representativeness of the observational network

To scale anthropogenic emissions, our approach consists of comparing observed and modeled concentrations and correcting emissions on the basis of this comparison. It is therefore essential to ensure that observed concentrations have a spatial representativeness consistent with the spatial resolution of the model. The number and spatial representativeness of the monitoring network's measurement stations are crucial to the proposed emission scaling approach. Internet platforms aggregating observations from different networks are providing a growing number of observations, mainly in urban agglomerations. A prerequisite for the approach is the analysis of the spatial representativeness of the monitoring network, in order to be consistent with model resolution.

## 2.3 Scaling of the anthropogenic emissions

The anthropogenic emission scaling approach relies on comparing observed versus modeled concentration ratios, with correction factors (CF) derived from these comparisons to adjust anthropogenic emissions for each pollutant. This approach assumes that biases between observed and modeled concentrations in urban agglomerations are primarily due to biases in anthropogenic emission inventories. Temporally, emission scaling is based on a comparison of modeled and observed concentrations averaged over the last few days. Averaging only the last week allows rapid variations in emissions to be captured, for example during events such as COVID-19 or other special events. A time scale of less than a week mixes weekdays and weekends, and is therefore inconsistent. Spatially, emission scaling can be carried out locally around a station, for a limited spatial area, or for an entire urban agglomeration if anthropogenic emissions can be considered uniform.

The approach consists of two complementary emission scaling calculations, based on daily or hourly concentrations averaged over the last week. CF are calculated weekly for NO<sub>x</sub>, SO<sub>2</sub>, CO, PM<sub>2.5</sub> and PM<sub>10</sub> to provide daily or hourly emission-scaled forecasts. For VOC, CF are determined based on modeled O<sub>3</sub> biases, assuming a NO<sub>x</sub>-saturated regime. Three regional forecasts are initiated daily, each differing in their anthropogenic emissions:

- 173 • F-REF (reference forecast),
- 174 • F-DAY (daily emission-scaled forecast),
- 175 • F-HOUR (hourly emission-scaled forecast).

### 176 **2.3.1 Correction factors of NO<sub>x</sub>, SO<sub>2</sub>, CO, PM<sub>2.5</sub> and PM<sub>10</sub>**

177 Correction factors (CF) are calculated for NO<sub>x</sub>, SO<sub>2</sub>, CO, PM<sub>2.5</sub> and PM<sub>10</sub>.

178 (i) With the daily emission-scaled forecast, a single CF-daily is calculated based  
179 on the ratio of the observed and modeled weekly concentration averages (WCA):

$$CF - daily(w) = \frac{WCA_{obs}(w-1)}{WCA_{mod}(w-1)} \quad (1)$$

180 Where  $w$  represents a given week.

181 (ii) With the hourly emission-scaled forecast, 24 CF-hourly are calculated based  
182 on the ratio of the observed and modeled weekly concentration averages per hour (WCAH):

$$CF - hourly(w, h) = \frac{WCAH_{obs}(w-1, h)}{WCAH_{mod}(w-1, h)} \quad (2)$$

183 Where  $h$  represents a given hour.

### 184 **2.3.2 Correction factor of VOC**

185 There are no routine observations of VOC concentrations due to the difficulty in  
186 measuring their various components, so information about VOC comes primarily from  
187 observational field campaigns (Theloke & Friedrich, 2007). As a result, VOC emissions  
188 from global anthropogenic inventories may not accurately reflect the reality of most megac-  
189 ities (Sokhi et al., 2022). Consequently, we propose to determine VOC-CF based on mod-  
190 eled O<sub>3</sub> biases.

191 O<sub>3</sub> is a secondary pollutant formed during the day, depending on the relative amounts  
192 of VOC and NO<sub>x</sub> (e.g. Monks et al., 2015). Assuming a NO<sub>x</sub>-saturated regime, the pro-  
193 duction of O<sub>3</sub> is controlled by the VOC concentration. Therefore, if the modeled O<sub>3</sub> con-  
194 centration is overestimated, it implies an overestimation in VOC, and conversely for an  
195 underestimation. Based on this assumption, a single CF is calculated for VOC emissions  
196 based on the ratio of the observed and modeled maximum O<sub>3</sub> concentration (MaxO<sub>3</sub>)  
197 of the hourly average diurnal cycle of the previous week:

$$CF - daily(w) = \frac{MaxO3_{obs}(w-1)}{MaxO3_{mod}(w-1)} \quad (3)$$

198 As NO<sub>x</sub>-CF differs for F-DAY and F-HOUR, the modeled O<sub>3</sub> concentrations are  
199 expected to be different, resulting in different VOC-CF.

200 After several weeks, the evolution of the correction factors for both daily and hourly  
201 approaches, along with their impact on statistical performance, is analyzed. This infor-  
202 mation is then interpreted to adjust the inventory of anthropogenic emissions used for  
203 the regional forecasts in terms of magnitude and hourly profiles.

## 204 **2.4 Limitations of observation-based emission scaling**

- 205 • NO<sub>x</sub>

206 For NO<sub>x</sub>, composed of NO and NO<sub>2</sub>, the emissions scaling approach should be ef-  
207 fective due to their short lifetimes. However, their links with O<sub>3</sub> chemistry lead to high

208 diurnal variability in NO<sub>x</sub> concentrations. Moreover, the spatial representativeness of  
 209 the monitoring network could lead to inaccurate CF, especially for NO.

- 210 • SO<sub>2</sub>

211 The SO<sub>2</sub> emission scaling approach is also expected to be efficient due to its short  
 212 lifetime, although conversion to sulfate may affect modeled PM<sub>2.5</sub> and PM<sub>10</sub> concentra-  
 213 tions.

- 214 • CO

215 The CO emission scaling approach may be less efficient due to its longer lifetime  
 216 (much longer than NO<sub>x</sub> and SO<sub>2</sub>), which could result in a large influence of CO trans-  
 217 ported from outside the urban agglomeration.

- 218 • PM<sub>2.5</sub> and PM<sub>10</sub>

219 PM<sub>2.5</sub> and PM<sub>10</sub> are composed of carbonaceous, inorganic, mineral, and marine  
 220 aerosols, which vary widely in urban agglomerations (e.g. Cheng et al., 2016). In addi-  
 221 tion, secondary organic and inorganic aerosols are formed in the atmosphere depending  
 222 on the amount of gaseous precursors and meteorological conditions (e.g. Zhang et al.,  
 223 2009). For aerosols (*i.e.* PM<sub>2.5</sub> and PM<sub>10</sub>), the emission scaling approach is expected  
 224 to be limited because of the complexity of their composition and relationships with gaseous  
 225 precursors, and because of the transport of aerosols from outside the agglomeration.

- 226 • VOC

227 To correct VOC emissions, an additional assumption is necessary regarding the chem-  
 228 ical regime, which must be NO<sub>x</sub>-saturated for the VOC-CF to be efficient. Therefore,  
 229 it is essential to verify this assumption, which can be achieved through indicators of the  
 230 chemical regime (Liang et al., 2006). These indicators are concentration ratios of chem-  
 231 ical species associated with the formation of tropospheric O<sub>3</sub> through cycling chain re-  
 232 actions involving OH, HO<sub>2</sub>, and RO<sub>2</sub> (Levy, 1971). Zhang et al. (2009) discuss the ro-  
 233 bustness of these indicators and demonstrate their consistency when the chemical regime  
 234 is well established. Among the different indicators, only O<sub>3</sub> / NO<sub>x</sub> can be studied for  
 235 both observations and forecasted concentrations. A NO<sub>x</sub>-saturated regime is well defined  
 236 by the O<sub>3</sub> / NO<sub>x</sub> indicator when the value is below 15 (Zhang et al., 2009). The VOC  
 237 emission scaling approach may enable the modeled chemical regime to be more consis-  
 238 tent with the observations.

### 239 **3 Regional forecasts for São Paulo, Brazil**

#### 240 **3.1 Methodology applied to São Paulo**

241 The regional forecasts were initiated on 30 January 2023, and the assessment cov-  
 242 ers the period from 6 February to 17 April 2023. This period includes the São Paulo Car-  
 243 nival (11-19 February), which may have an impact on anthropogenic emissions.

244 The choice to focus on São Paulo has been motivated by several factors: (i) its sta-  
 245 tus as South America's largest megacity, lacking a regional air quality forecast, (ii) the  
 246 presence of a high-quality monitoring network (Andrade et al., 2017), (iii) the variabil-  
 247 ity of the megacity's air quality due to high anthropogenic emissions, and (iv) modeled  
 248 air quality in São Paulo has been investigated by a model intercomparison (Deroubaix  
 249 et al., 2024).

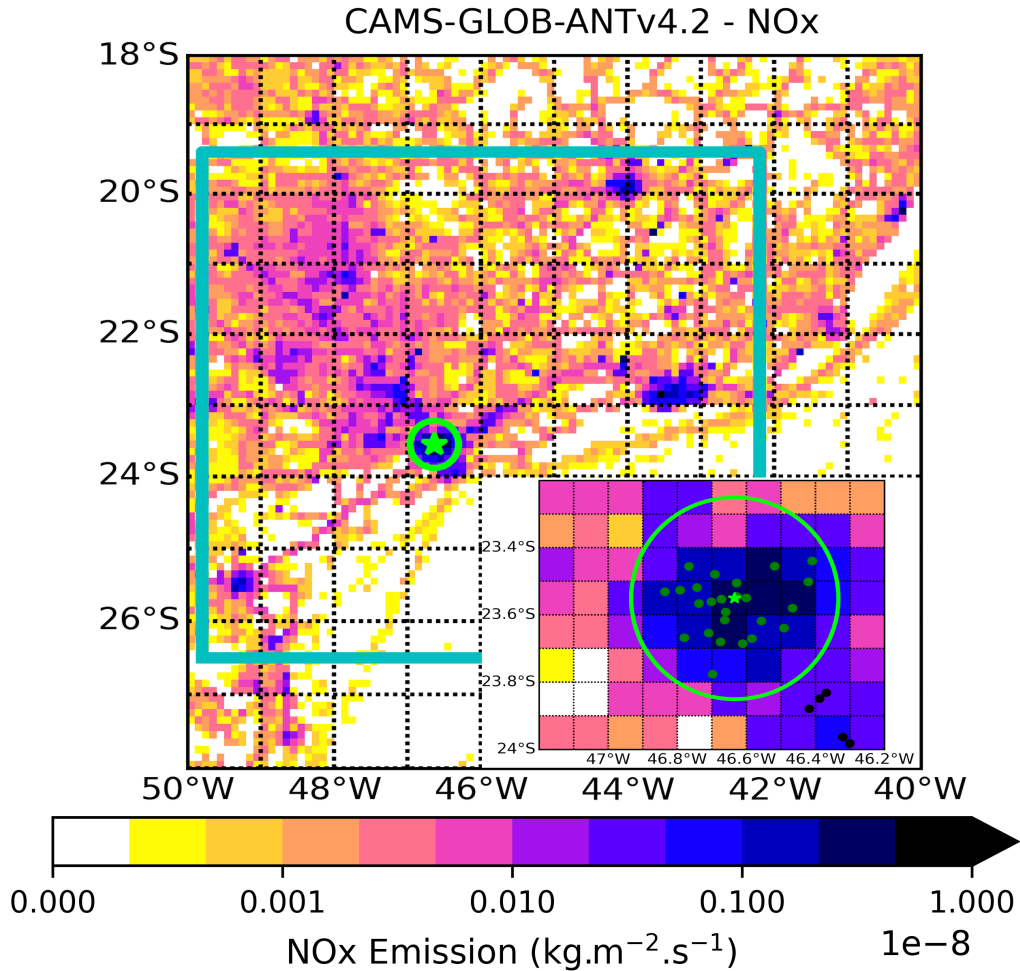


**Figure 1.** *NOx emission flux maps (sum of all sectors) for the São Paulo region from the CAMS-GLOB-ANTv4.2 anthropogenic inventory, with a zoom on the most densely populated area of the megacity (inside the green circle). The horizontal modeling domain used for regional forecasts corresponds to the blue rectangle. On the zoom (bottom right), the locations of the air quality monitoring network stations (dots) are shown, with the distinction of the 26 stations within the most densely populated area of the megacity (inside the green circle). São Paulo's traditional city center is located at the Cathedral da Sé (green star), which is used as the center of the 30-km radius circle.*

250 The horizontal modeling domain covers areas with high anthropogenic emissions,  
 251 and it includes a significant portion of the ocean in order to reproduce the land-sea breeze,  
 252 which play an important role in the pollutant transport and removal (Freitas et al., 2007).  
 253 NO<sub>x</sub> annual emission fluxes are depicted for the São Paulo region, along with the loca-  
 254 tions of the measurement stations (Figure 1). The monitoring network comprises 26 sta-  
 255 tions within a 30-km radius circle centered at São Paulo's traditional city center (Cat-  
 256 edral da Sé), ensuring adequate coverage of high NO<sub>x</sub> anthropogenic emission areas, reach-  
 257 ing up to  $2.3 \times 10^{-9} \text{ kg.m}^{-2}.\text{s}^{-1}$ .

### 258 3.2 Configuration of the daily regional forecasts

259 The regional forecasts use the WRFchem model (Grell et al., 2005; Fast et al., 2006;  
 260 Powers et al., 2017) combined with the WACCM6 (hereafter WACCM) forecast (Gettelman  
 261 et al., 2019) provided by NCAR (Table A1). The daily updated datasets include, for me-  
 262 teorology the FNL dataset from the US National Centers for Environmental Prediction  
 263 (NCEP, 2023), for fire emissions the FINNv1 dataset (Wiedinmyer et al., 2011) and for  
 264 chemical boundary conditions the WACCM forecasts (Gettelman et al., 2019). Five steps  
 265 are performed daily to produce the regional forecasts: (1) preprocessing of NCEP me-  
 266 teorological data, (2) calculation of fire, biogenic, and anthropogenic emissions, (3) in-  
 267 tegration of WACCM forecasts as chemical boundary conditions, (4) simulation of air  
 268 quality for the next two days with WRFchem, (5) interpolation of the forecasts at the  
 269 city center and comparison with air quality station data.

270 The modeling domain consists of a small horizontal grid of 80 x 80 cells with 37  
 271 vertical levels, which gives importance to the meteorological and chemical boundary con-  
 272 ditions (Table A1). The model configuration is close to that used by Deroubaix et al.  
 273 (2024), but the domain spatial resolution is reduced and without nested domain. The  
 274 resolution is 10 km, corresponding to the resolution of the anthropogenic emissions in-  
 275 ventory (Granier et al., 2019), with sectoral hourly profiles (Crippa et al., 2020), which  
 276 differ depending on weekdays (Figure A1). The chemical scheme is MOZART4 (Emmons  
 277 et al., 2010), and the aerosol scheme is GOCART (Chin et al., 2002), ensuring fast fore-  
 278 cast computation (Pfister et al., 2011). With this setup, the air quality forecast for the  
 279 next two days can be produced in about 2 hours using 40 processors. About 7 GB of data  
 280 are stored per day, which amounts to about 2.5 TB per year.

### 281 3.3 Spatial representativeness of the monitoring network

282 Observations are obtained from the OpenAQ data platform via an API (Applica-  
 283 tion Protocol Interface), which allows fast and portable data access (OPENAQ, 2023).  
 284 In order to derive the correction factors (CF) of anthropogenic emissions, a super-observation  
 285 of pollutant concentration in the city center is calculated from the measurement stations  
 286 of the São Paulo monitoring network for each pollutant. Different calculations of the super-  
 287 observation are possible to derive CF and to modify anthropogenic emissions (*cf.* Sec-  
 288 tion 2.2). The methodology of Deroubaix et al. (2024) is adapted to the location of the  
 289 stations in the São Paulo monitoring network in order to ensure the spatial representa-  
 290 tiveness of the super-observation corresponding to the entire megacity. The super-observation  
 291 used in this study is based on the measurement stations within a 30-km radius of the  
 292 city center (Figure 1). Using inverse distance weighting interpolation, the city super-observation  
 293 is calculated and compared to the forecasted concentrations interpolated at the city cen-  
 294 ter. From these comparisons, CF are derived for each pollutant. These CF, calculated  
 295 on Monday, are applied to anthropogenic emissions for the rest of the week. For NO<sub>x</sub>,  
 296 the CF are based only on the NO<sub>2</sub> concentration due to sparse NO data and its short  
 297 lifetime.

## 4 Forecast performance evaluation for São Paulo

The regional forecasts are evaluated for São Paulo for a 10-week period (6 February to 17 April 2023). The scaling of anthropogenic emissions is done on Mondays (*i.e.* the CF-daily and CF-hourly calculations). Thus, this section analyzes the evolution of the statistical performance from one week to the next, for NO<sub>x</sub> (Section 4.1), for SO<sub>2</sub>, CO, PM<sub>2.5</sub> and PM<sub>10</sub> (Section 4.2), and for VOC (Section 4.3).

First, the week-to-week evolution of the correction factors (CF) is studied during the 10-week period in order to determine if the CF converge to a value after some weeks. Second, the weekly evolutions of the statistical performance of the three regional forecasts are investigated for each pollutant using two statistical metrics (1) the model biases and (2) the root mean square error (RMSE). The difference in performance for the next day (d+1) and the day after (d+2) is also evaluated with the same statistical metrics, and compared to two global forecasts, the WACCM forecast (Gettelman et al., 2019) with a spatial resolution of about 100 km and the CAMS forecast (ECMWF, 2023) with a finer resolution of about 40 km (Table A1).

### 4.1 NO<sub>x</sub> emission scaling evaluation

We first focus on NO<sub>2</sub>, for which we expect the emission scaling approach to be efficient due to the short lifetime of NO<sub>2</sub>. Moreover, we choose to scale NO<sub>x</sub> emission using the CF calculated on NO<sub>2</sub>, thus NO<sub>2</sub>-CF are equivalent to NO<sub>x</sub>-CF. The NO<sub>2</sub>-CF used for the scaling of daily and hourly emissions are presented over the 10-week period (Figure 2-a).

With the daily emission scaling, NO<sub>x</sub> emissions are reduced by half in the first week. The CF value is  $\approx 0.5$ , and then this value varies slightly until the end of the period. With the hourly emission scaling, CF tends to decrease emissions during the night but increasing emissions during the day, leading to modifications of the hourly emission profile. The mean of hourly NO<sub>2</sub>-CF tend to be higher ( $\approx 0.8$ ) than daily NO<sub>2</sub>-CF (Figure A2).

From the first week evaluated (6 to 13 February), modeled NO<sub>2</sub> biases are reduced for both emission-scaled forecasts (Figure 2-b). The evolution of the statistical performance over the 10 weeks shows that both emission-scaled forecasts lead to a strong reduction in weekly NO<sub>2</sub> biases of  $\approx 20$  ppb compared to the reference. In addition, the RMSE is also reduced by  $\approx 10$  ppb compared to the reference (Figure A2). The forecasts produced for d+1 and for d+2 are similar in terms of bias and RMSE for all forecasts. The daily and hourly emission-scaled forecasts lead to lower biases and RMSE than the two global forecasts and the reference (Figure A2).

Both regional emission-scaled forecasts are based on modeled biases averaged over the last week. The average hourly diurnal cycles are examined because the emission-scaled forecasts are expected to be in better agreement with observations than the reference forecast (F-REF) from the first week evaluated (Figure 3).

The modeled NO<sub>2</sub> concentration is underestimated during the day and overestimated during the night for both F-DAY and F-REF. Although the biases for daily emission-scaled forecast (F-DAY) are increased during the day compared to the reference forecast (F-REF), the diurnal cycle of the modeled NO<sub>2</sub> is improved in magnitude as there is a strong reduction in biases of up to 20 ppb during the night. With the hourly emission-scaled forecast (F-HOUR), the hourly mean diurnal cycle is improved for each hour compared to F-REF. There is a large reduction in bias during the night (up to 25 ppb) compared to F-REF, which is a negligible bias during the day. Consequently, this scaling, which modifies the hourly emission profile, leads to the best agreement with observations. Nevertheless, there is an overestimation of NO<sub>2</sub> concentrations in the morning at 09:00 and in the evening at 18:00, two hours later than the traffic emission peaks at 07:00 in



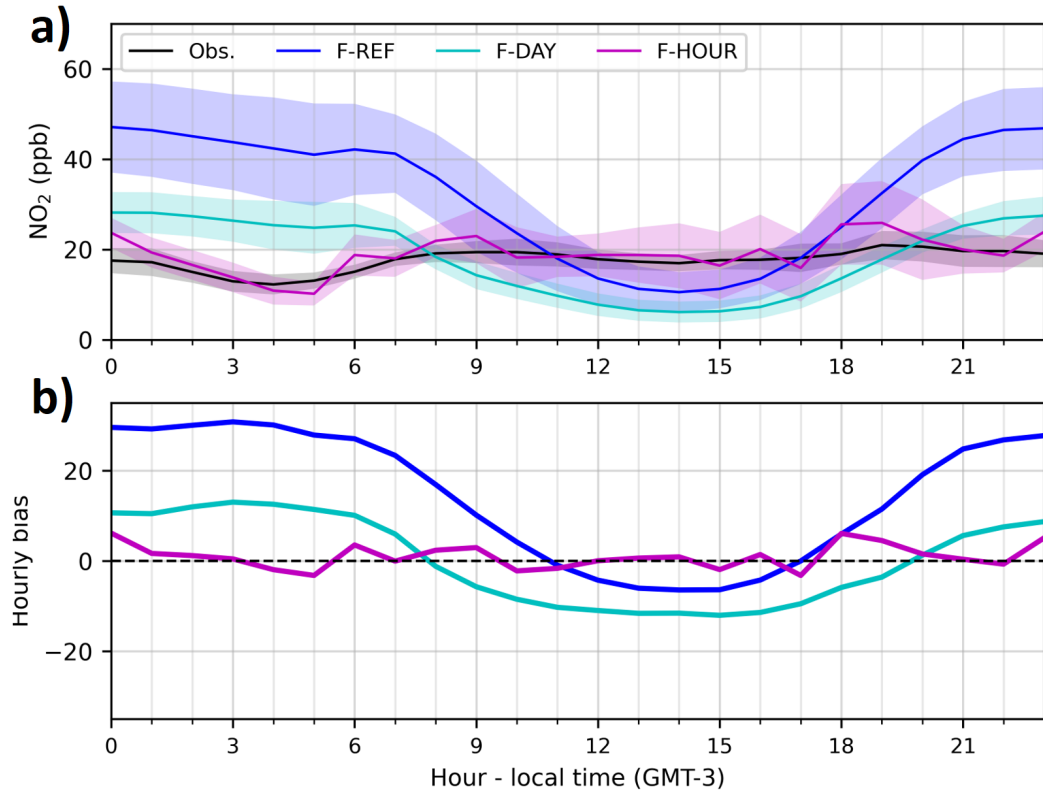


**Figure 3.** (a) Average hourly diurnal cycles of observed and forecasted NO<sub>2</sub> concentrations from the second week to the end of the 10-week period (13 February to 17 April 2023) in the center of São Paulo. Modeled concentrations correspond to the three regional forecasts: (i) F-REF, the reference forecast, (ii) F-HOUR, the hourly emission-scaled forecast, and (iii) F-DAY, the daily emission-scaled forecast. The color shades correspond to the standard deviation of the concentrations for each hour of the period. (b) Average hourly biases of the three regional forecasts, which are the differences in the average hourly diurnal cycles of observed and modeled NO<sub>2</sub> concentrations (shown in panel a).

the morning and 16:00 in the evening prescribed in the model (Figure A1). The CF of these hours do not tend to converge after 10 weeks, while the CF of the other hours tend to a clear value (Figure 2-a). This result suggests that the hourly emission scaling compensates for biases that are not solely related to the hourly profiles of anthropogenic emissions, such as a poor representation of the height of the urban boundary layer, which changes rapidly in the morning and evening, and which could be related to the absence of the urban heat island effect in the model, leading to an underestimated height (Deroubaix et al., 2024).

Although the approach is limited by the allocation to different sectors in the anthropogenic emission inventories, the CF tend to 0.5 for the daily emission-scaled forecast and 0.8 for the hourly one, so the NO<sub>x</sub> anthropogenic emissions from the used inventory should be reduced in São Paulo. This reduction of the emission in the center of São Paulo is in agreement with the previous study of Vivanco and de Fatima Andrade (2008). In addition, hourly CF increase during the day and decrease at night, so hourly emission profiles should be modified accordingly, but the CF obtained for morning and evening should be taken with caution. In conclusion, regional forecasts with the emission scaling approach reduce the mean weekly NO<sub>2</sub> bias, and the reduction is similar for the daily and hourly emission-scaled forecasts. However, only the hourly emission-scaled forecast leads to a better representation of the average hourly diurnal NO<sub>2</sub> cycles, suggesting that the hourly emissions profiles could be revised using hourly CF information.

#### 4.2 SO<sub>2</sub>, CO, PM<sub>2.5</sub> and PM<sub>10</sub> emission scaling evaluations

Deroubaix et al. (2024) have shown that SO<sub>2</sub> concentration is largely overestimated by air quality models in central São Paulo in 2019. For both emission-scaled forecasts, SO<sub>2</sub>-CF are reduced from the first week and then tend towards a value of  $\approx 0.1$  (Figure 4-a). Except for the 05:00 correction factor, we note that the SO<sub>2</sub>-CF increases from the third week to the end of the period, reaching a value of 4. This result reflects a problem with the calibration of the measuring instruments, which were all carried out at the same time, except for one station close to the SO<sub>2</sub> sources. The bias therefore changes during this hour, due to the problem of spatial representativeness of this station for the megacity.

The evolution of weekly mean SO<sub>2</sub> biases for the three regional simulations and the two global forecasts shows that the reference simulation has the largest bias (Figure 4-b). The CAMS and WACCM forecasts have biases of  $\approx 5$  ppb, while F-REF reaches 20 ppb. Both F-DAY and F-HOUR significantly reduce biases, which tend towards 0 at the end of the period. In addition, the mean bias and RMSE of SO<sub>2</sub> are reduced in the same proportions for d+1 and for d+2 (Figure A3). Consequently, with emission scaling approach, regional forecasts of SO<sub>2</sub> are in good agreement with observations in terms of temporal variability.

Compared to NO<sub>2</sub> and SO<sub>2</sub>, CO has a longer lifetime, so the influence of emission sources outside São Paulo, which are not affected by the anthropogenic emission scaling, is stronger. The daily emission-scaled forecast for CO leads to a CF with a value of  $\approx 0.5$  from the first week to the end of the period (Figure 4-c), which is also the case for the mean hourly CO-CF (Figure A4). With the hourly emission-scaled forecast, CO-CF associated with the hours from 11:00 to 05:00 are reduced beyond the value obtained with the daily CF, while for the other hours, CO-CF are increased. CF are even higher than 1 in the morning and evening for hours associated with peak traffic emissions. Over the 10-week period, the F-REF and CAMS overestimate CO by  $\approx 0.1$  ppm, while WACCM underestimates CO by  $\approx 0.2$  ppm (Figure 4-d). Both F-DAY and F-HOUR lead to small biases from the fourth week of the period onwards. For both forecasts, the RMSE is reduced by  $\approx 0.1$  ppm compared with F-REF for d+1 and also for d+2. As a result, the temporal variability of CO concentration is improved with the emission scaling approach

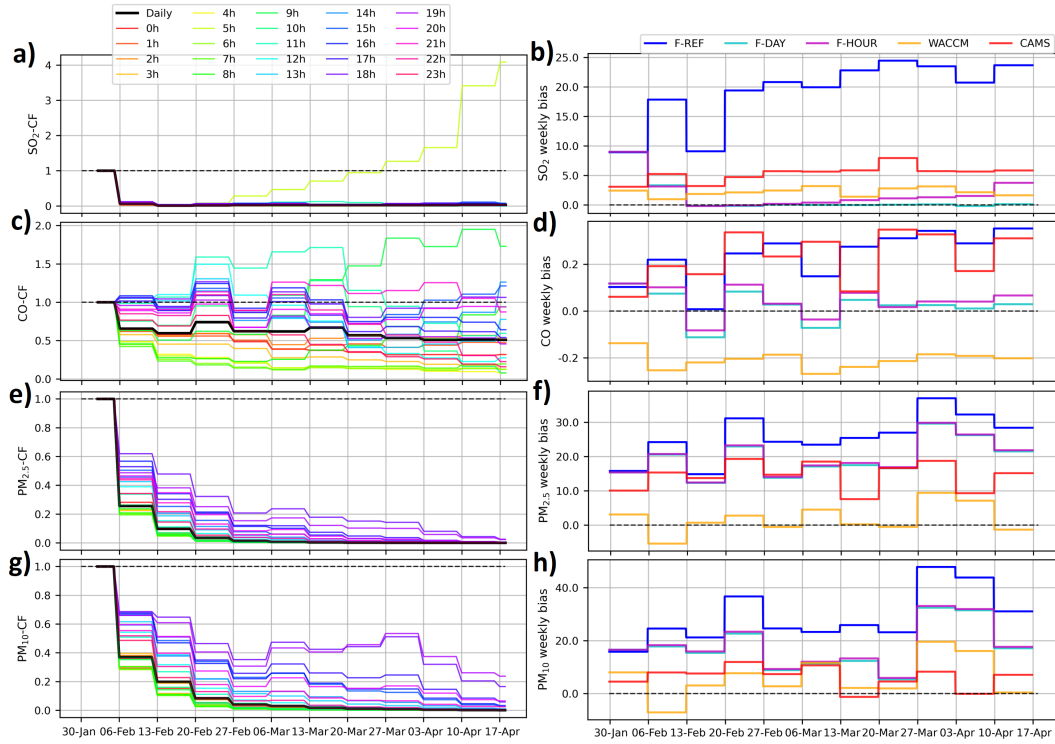


**Figure 4.** Weekly evolution of (a, c, e and g) daily and hourly correction factors (CF) for CO, SO<sub>2</sub>, PM<sub>2.5</sub> and PM<sub>10</sub> used for the daily and hourly emission-scaled forecasts (F-DAY and F-HOUR) of a given week, and (b, d, f and h) mean biases of forecasted concentrations of SO<sub>2</sub> (in ppb), CO (in ppm), PM<sub>2.5</sub> and PM<sub>10</sub> (in  $\mu\text{g}\cdot\text{m}^{-3}$ ), for the three regional forecasts (F-REF, F-DAY and F-HOUR), and for the two global forecasts: (iv) WACCM provided by NCAR and (v) CAMS provided by ECMWF, over the 10-week period (in 2023) in the center of São Paulo. Hours are given in local time (GMT-3).

398 in center of São Paulo. However, the RMSE is greater than 0.1 ppm for all forecasts, sug-  
 399 gesting that some emission sources are missing or their intensities are inaccurate (Fig-  
 400 ure A4).

401 Investigating the PM forecasts, the anthropogenic emissions are largely reduced af-  
 402 ter three weeks, as CF tend towards a very low value below 0.2 for both emission-scaled  
 403 forecasts from week 4 to the end of the period (Figure 4-e and g). This leads to the strong  
 404 reduction of anthropogenic PM emissions in the center of the megacity from week 4 on-  
 405 wards. Weekly PM biases are reduced with the same intensity for both F-DAY and F-  
 406 HOUR from week 4 onwards (Figure 4-f and h). Thereafter, there is no significant change  
 407 in mean bias. Compared with the F-REF, the biases for  $\text{PM}_{2.5}$  are reduced by  $\approx 5 \mu\text{g}\cdot\text{m}^{-3}$   
 408 and by  $\approx 10 \mu\text{g}\cdot\text{m}^{-3}$  for  $\text{PM}_{10}$ . CAMS overestimates  $\text{PM}_{2.5}$  by  $\approx 10 \mu\text{g}\cdot\text{m}^{-3}$ , while for  
 409  $\text{PM}_{10}$  the bias is less than  $\approx 5 \mu\text{g}\cdot\text{m}^{-3}$ . The two global forecasts have the lowest biases  
 410 and RMSE for  $\text{PM}_{2.5}$  and  $\text{PM}_{10}$ . In addition, the three regional forecasts have lower sta-  
 411 tistical performances than the two global forecasts, with no difference between d+1 and  
 412 d+2 (Figures A5 and A6).

413 Although PM-CF is very low and therefore anthropogenic emissions are largely re-  
 414 duced, model biases remain positive. This overestimation of PM suggests that the model  
 415 overestimates the proportion of PM transported from outside the center of São Paulo.  
 416 Considering the hourly emission-scaled forecast, PM-CF for evening hours are higher than  
 417 those for other hours, showing that model biases are lower than during the rest of the  
 418 day, suggesting that anthropogenic PM contributes significantly to total evening PM.  
 419 Furthermore, if we compare  $\text{PM}_{2.5}$  and  $\text{PM}_{10}$ , we find that the correction factor for  $\text{PM}_{2.5}$   
 420 is stronger during the day ( $\approx 0.1$ ) than that for  $\text{PM}_{10}$  ( $\approx 0.2$ ), which may be linked to  
 421 an overestimation of secondary aerosol production.

### 422 4.3 VOC emission scaling evaluation

423 For São Paulo, Deroubaix et al. (2024) have shown that a regional simulation us-  
 424 ing a local anthropogenic inventory and without biogenic emissions reproduces the  $\text{O}_3$   
 425 concentration in good agreement with observations, challenging the values of global an-  
 426 thropogenic inventories that have significant VOC emissions in the center of the megac-  
 427 ity. Using the emission scaling approach for VOC under the assumption that the regime  
 428 is saturated with NOx (*i.e.* controlled by the VOC concentration), the bias of the max-  
 429 imum daily  $\text{O}_3$  concentration should be reduced as the approaches modify the chemi-  
 430 cal regime compared to the reference forecast, which depends on the NOx / VOC ratio.

431 VOC-CF are largely reduced from the first week for both F-DAY and F-HOUR,  
 432 and tend to be less than 0.1 from the sixth week onwards (Figure 5-a). This result in-  
 433 dicates that the modeled daily maximum of  $\text{O}_3$  is overestimated during the first five weeks  
 434 of the period for both emission-scale forecasts. As NOx-CF are different for the two emission-  
 435 scaled forecasts, this leads to different changes in the ratio between NOx-CF and VOC-  
 436 CF (*cf.* Section 2.3). The change in NOx emissions is greater with the daily CF (NOx-  
 437 CF  $\approx 0.5$ ) than with the hourly CF (NOx-CF  $\approx 0.8$ ). As a result, the NOx-CF / VOC-  
 438 CF ratios increase over the 10-week period, reaching a value of  $\approx 30$  for the hourly CF  
 439 and  $\approx 120$  for the daily CF. Therefore, NOx emissions decrease much less than VOC emis-  
 440 sions for both emission-scale forecasts. This analysis of the evolution of VOC-CF ver-  
 441 sus NOx-CF supports the assumption of a NOx-saturated regime in center of São Paulo.

442 To verify the assumption of a NOx-saturated regime, the  $\text{O}_3$  / NOx ratio is stud-  
 443 ied for both observations and regional forecasts (Figure 5-b). A value of this ratio of less  
 444 than 15 is associated with a NOx-saturated regime (Zhang et al., 2009). The scaling of  
 445 VOC emissions does not result in a modeled  $\text{O}_3$  / NOx ratio for F-DAY and F-HOUR  
 446 that is more consistent with the observed variability than F-REF. However, the observed  
 447 and modeled values are clearly associated with a NOx-saturated regime, confirming that  
 448 the assumption is appropriate for São Paulo (over the period studied).

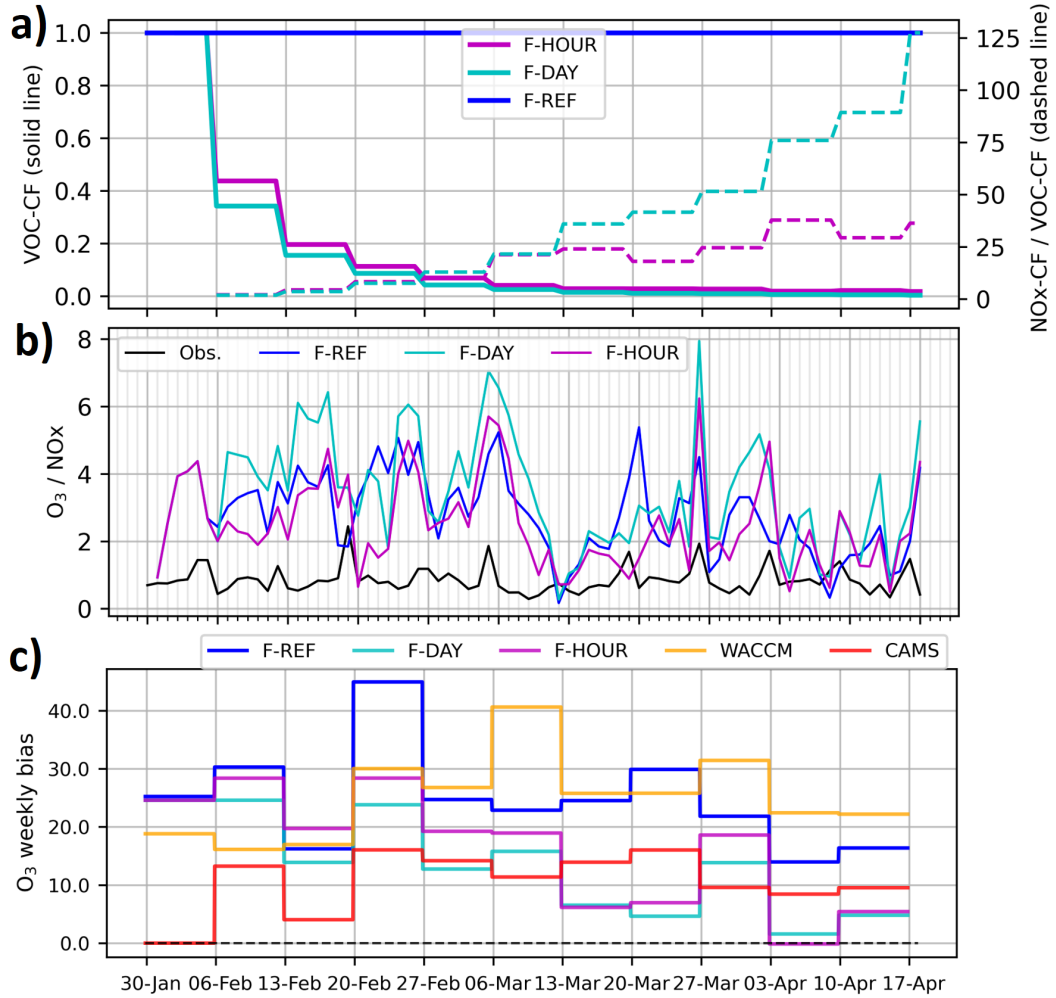


**Figure 5.** Weekly evolution of (a) VOC correction factors (CF) used for the daily and hourly emission-scaled forecasts (F-DAY and F-HOUR) of a given week together with the NO<sub>x</sub>-CF / VOC-CF ratio, (b) O<sub>3</sub> / NO<sub>x</sub> ratio for the observation and the three regional forecasts (F-REF, F-DAY and F-HOUR), and (c) mean biases of O<sub>3</sub> forecasted concentrations, for the three regional forecasts (F-REF, F-DAY and F-HOUR), and for the two global forecasts: (iv) WACCM provided by NCAR and (v) CAMS provided by ECMWF, over the 10-week period (in 2023) in the center of São Paulo.

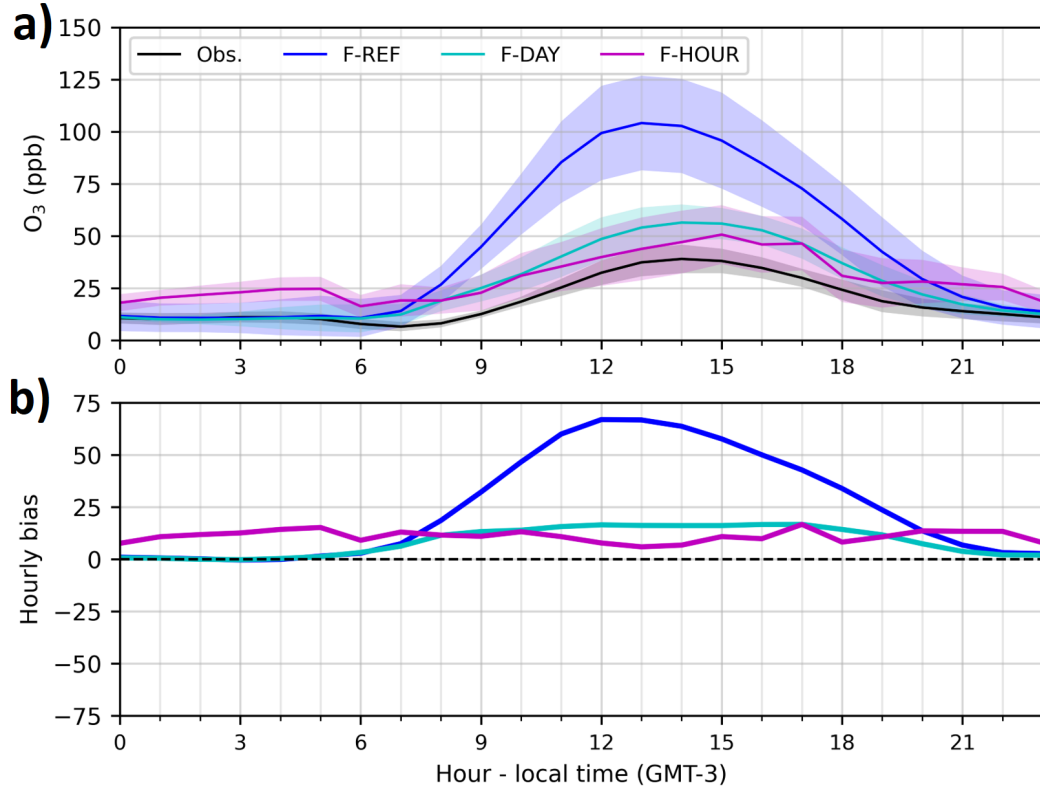


**Figure 6.** (a) Average hourly diurnal cycles of observed and modeled O<sub>3</sub> concentrations from the sixth week to the end of the 10-week period (13 March to 17 April 2023) in the center of São Paulo. Modeled concentrations correspond to the three regional forecasts: (i) F-REF, the reference forecast, (ii) F-HOUR, the hourly emission-scaled forecast, and (iii) F-DAY, the daily emission-scaled forecast. The color shades correspond to the standard deviation of the concentrations for each hour of the period. (b) Average hourly biases of the three regional forecasts, which are the differences in the average hourly diurnal cycles of observed and modeled O<sub>3</sub> concentrations (shown in panel a).

449 Over the 10-week period, the statistical performance for O<sub>3</sub> of F-REF is lower than  
 450 the CAMS global forecast and comparable to the WACCM forecast both in terms of mean  
 451 weekly bias (Figure 5-c) and RMSE (Figure A7). For both emission-scaled forecasts, a  
 452 significant reduction in mean weekly bias and RMSE is observed after five weeks, whereas  
 453 the reduction in NO<sub>x</sub>-CF is reached after two weeks (*cf.* Section 4.1). From the sixth  
 454 week of the period onwards, F-DAY and F-HOUR have the best statistical performance  
 455 for O<sub>3</sub> for the next day (d+1) and the day after (d+2), both in terms of mean weekly  
 456 bias (Figure 5-c) and RMSE (Figure A7).

457 We examine the changes in average hourly diurnal cycles obtained between the sixth  
 458 week and the end of the 10-week period. F-REF overestimates O<sub>3</sub> concentrations dur-  
 459 ing the day (06:00 to 21:00), while the daytime O<sub>3</sub> bias is reduced by more than 25 ppb  
 460 for both emission-scaled forecasts. The best agreement is obtained with F-DAY, because  
 461 F-HOUR leads to an overestimation of O<sub>3</sub> concentrations at night. These results sug-  
 462 gest that not only the magnitude of anthropogenic emissions and hourly profiles need  
 463 to be revised, but also that the reduction in NO<sub>x</sub> emissions at night is too strong for F-  
 464 HOUR, which again points to an underestimation of the urban boundary layer height  
 465 at night due to the absence of the urban heat island effect in the model.

## 466 5 Conclusions

467 In this study, we present a new approach to improve air quality forecasts in urban  
 468 agglomerations using observation-based scaling of anthropogenic emissions. The proposed  
 469 approach assumes that in large urban agglomerations, such as megacities, biases between  
 470 observed and modeled concentrations arise mainly from biases in anthropogenic emis-  
 471 sions. The approach consists in deriving daily and hourly correction factors for NO<sub>x</sub>, SO<sub>2</sub>,  
 472 CO, PM<sub>2.5</sub> and PM<sub>10</sub> based on the comparison of observed and modeled concentration  
 473 ratios using daily and hourly averages respectively. For VOC, the emission scaling is de-  
 474 termined on the basis of modeled O<sub>3</sub> biases during the day, assuming a NO<sub>x</sub>-saturated  
 475 regime.

476 The implementation of the approach in São Paulo shows that a substantial reduc-  
 477 tion of anthropogenic NO<sub>x</sub> emissions is required. The hourly emission-scaled forecast sig-  
 478 nificantly improves NO<sub>2</sub> concentration forecasts compared to the daily emission-scaled  
 479 forecast, indicating that both the magnitude and hourly emission profile can be refined  
 480 using information obtained over a 10-week period. In addition, ozone concentrations are  
 481 improved over the study period by correcting for VOC emissions, with adjustments made  
 482 under the validated assumption of a NO<sub>x</sub>-saturated chemical regime in the center of São  
 483 Paulo. The approach also performs well for SO<sub>2</sub> and CO, while improvements for PM  
 484 are limited due to the transport of biomass burning aerosols and secondary aerosol for-  
 485 mation.

486 The implementation of this approach for regional forecasts (or the analysis of a past  
 487 period) provides valuable insights within a short timeframe and informs further needed  
 488 adjustments to anthropogenic emission magnitudes and temporal emission profiles. How-  
 489 ever, the accuracy of the observation-based emission scaling is limited by four key fac-  
 490 tors: (i) the modeling of the urban meteorology, (ii) the spatial representativeness of the  
 491 monitoring network, (iii) the transport of pollutants from outside the urban agglomera-  
 492 tion, and (iv) the links between primary trace gases that are precursors of secondary  
 493 organic or inorganic aerosols.

494 In conclusion, the proposed approach to improve regional forecasts can be tested  
 495 and implemented in other urban areas. For a specific urban agglomeration, the approach  
 496 provides valuable top-down constraints to bottom-up global anthropogenic emission in-  
 497 ventories and improves regional air quality forecasts.

498 **Open Research Section**

499 Availability of the data: The observed and forecasted pollutant concentrations an-  
500 alyzed in this study are available through this web link: [https://zenodo.org/records/](https://zenodo.org/records/10977856)  
501 10977856, last access: April 16, 2024 [Dataset].

502 **Acknowledgments**

503 AD acknowledges the European Union's Horizon 2020 research and innovation pro-  
504 gramme for supporting this work under the Marie Skłodowska-Curie grant agreement  
505 No 895803 (MACSECH — H2020-MSCA-IF-2019).

506 This article is a direct contribution to the research themes of the Klimapolis Lab-  
507 oratory (klimapolis.net), which is funded by the German Federal Ministry of Education  
508 and Research (BMBF).

509 GB acknowledges the National Center for Atmospheric Research, which is spon-  
510 sored by the US National Science Foundation.

511 // Authors contribution:

512 AD designed the study, performed the analysis and wrote the first draft. All au-  
513 thors contributed to the final version of the manuscript.

514 The authors gratefully acknowledge the resources of the Deutsches Klimarechen-  
515 zentrum (DKRZ) granted by its Scientific Steering Committee (WLA) under project ID  
516 bm1257.

517 **References**

- 518 Andrade, M. d. F., Kumar, P., de Freitas, E. D., Ynoue, R. Y., Martins, J., Mar-  
519 tins, L. D., . . . Zhang, Y. (2017, 6). Air quality in the megacity of são paulo:  
520 Evolution over the last 30 years and future perspectives. *Atmospheric Environ-*  
521 *ment*, 159, 66-82. doi: 10.1016/j.atmosenv.2017.03.051
- 522 Baklanov, A., Molina, L. T., & Gauss, M. (2016). Megacities, air quality and cli-  
523 mate. *Atmospheric Environment*, 126, 235-249. doi: 10.1016/j.atmosenv.2015  
524 .11.059
- 525 Bocquet, M., Elbern, H., Eskes, H., Hirtl, M., Žabkar, R., Carmichael, G. R.,  
526 . . . Seigneur, C. (2015, 5). Data assimilation in atmospheric chemistry  
527 models: current status and future prospects for coupled chemistry meteo-  
528 rology models. *Atmospheric Chemistry and Physics*, 15, 5325-5358. doi:  
529 10.5194/acp-15-5325-2015
- 530 Brasseur, G. P., & Jacob, D. J. (2017). *Modeling of atmospheric chemistry*. Cam-  
531 bridge University Press.
- 532 Brasseur, G. P., Xie, Y., Petersen, A. K., Bouarar, I., Flemming, J., Gauss, M., . . .  
533 Zhou, G. (2019, 1). Ensemble forecasts of air quality in eastern China-Part  
534 1: Model description and implementation of the MarcoPolo-Panda predic-  
535 tion system, version 1. *Geoscientific Model Development*, 12, 33-67. doi:  
536 10.5194/gmd-12-33-2019
- 537 Carmichael, G. R., Sandu, A., Chai, T., Daescu, D. N., Constantinescu, E. M., &  
538 Tang, Y. (2008, 3). Predicting air quality: Improvements through advanced  
539 methods to integrate models and measurements. *Journal of Computational*  
540 *Physics*, 227, 3540-3571. doi: 10.1016/j.jcp.2007.02.024
- 541 Carrassi, A., Bocquet, M., Bertino, L., & Evensen, G. (2018, 9). Data assimilation in  
542 the geosciences: An overview of methods, issues, and perspectives. *WIREs Cli-*  
543 *mate Change*, 9. doi: 10.1002/wcc.535
- 544 Castell, N., Dauge, F. R., Schneider, P., Vogt, M., Lerner, U., Fishbain, B., . . .

- 545 Bartonova, A. (2017, 2). Can commercial low-cost sensor platforms contribute  
546 to air quality monitoring and exposure estimates? *Environment International*,  
547 99, 293-302. doi: 10.1016/j.envint.2016.12.007
- 548 Cheng, Z., Luo, L., Wang, S., Wang, Y., Sharma, S., Shimadera, H., ... Hao,  
549 J. (2016, 4). Status and characteristics of ambient pm2.5 pollution in  
550 global megacities. *Environment International*, 89-90, 212-221. doi:  
551 10.1016/j.envint.2016.02.003
- 552 Chin, M., Ginoux, P., Kinne, S., Torres, O., Holben, B. N., Duncan, B. N., ...  
553 Nakajima, T. (2002, 2). Tropospheric aerosol optical thickness from the  
554 gocart model and comparisons with satellite and sun photometer mea-  
555 surements. *Journal of the Atmospheric Sciences*, 59, 461-483. doi:  
556 10.1175/1520-0469(2002)059<0461:TAOTFT>2.0.CO;2
- 557 Crippa, M., Solazzo, E., Huang, G., Guizzardi, D., Koffi, E., Muntean, M., ...  
558 Janssens-Maenhout, G. (2020, 12). High resolution temporal profiles in  
559 the emissions database for global atmospheric research. *Scientific Data*, 7, 121.  
560 doi: 10.1038/s41597-020-0462-2
- 561 Deroubaix, A., Brasseur, G., Gaubert, B., Labuhn, I., Menut, L., Siour, G., & Tuc-  
562 cella, P. (2021, 5). Response of surface ozone concentration to emission reduc-  
563 tion and meteorology during the covid-19 lockdown in europe. *Meteorological*  
564 *Applications*, 28. doi: 10.1002/met.1990
- 565 Deroubaix, A., Hoelzemann, J. J., Ynoue, R. Y., de Almeida Albuquerque, T. T.,  
566 Alves, R. C., de Fatima Andrade, M., ... Brasseur, G. (2024, 1). Intercom-  
567 parison of air quality models in a megacity: Toward an operational ensemble  
568 forecasting system for são paulo. *Journal of Geophysical Research: Atmo-*  
569 *spheres*, 129. doi: 10.1029/2022JD038179
- 570 Doumbia, T., Granier, C., Elguindi, N., Bouarar, I., Darras, S., Brasseur, G., ...  
571 Wang, T. (2021, 8). Changes in global air pollutant emissions during the  
572 covid-19 pandemic: a dataset for atmospheric modeling. *Earth System Science*  
573 *Data*, 13, 4191-4206. doi: 10.5194/essd-13-4191-2021
- 574 ECMWF. (2023). Copernicus atmosphere monitoring service, [dataset]. *Eu-*  
575 *ropean Center for Medium-Range Weather Forecasts*. Retrieved from  
576 [https://ads.atmosphere.copernicus.eu/cdsapp#!/dataset/cams-global](https://ads.atmosphere.copernicus.eu/cdsapp#!/dataset/cams-global-atmospheric-composition-forecasts)  
577 [-atmospheric-composition-forecasts](https://ads.atmosphere.copernicus.eu/cdsapp#!/dataset/cams-global-atmospheric-composition-forecasts), [Accessed:08/11/2023]
- 578 Emmons, L. K., Schwantes, R. H., Orlando, J. J., Tyndall, G., Kinnison, D., Lamar-  
579 que, J. F., ... Pétron, G. (2020, 4). The chemistry mechanism in the commu-  
580 nity earth system model version 2 (cesm2). *Journal of Advances in Modeling*  
581 *Earth Systems*, 12. doi: 10.1029/2019MS001882
- 582 Emmons, L. K., Walters, S., Hess, P. G., Lamarque, J.-F., Pfister, G. G., Fillmore,  
583 D., ... Kloster, S. (2010). Geoscientific model development description  
584 and evaluation of the model for ozone and related chemical tracers, version 4  
585 (mozart-4). *Geosci. Model Dev*, 3, 43-67.
- 586 Fast, J. D., Gustafson, W. I., Easter, R. C., Zaveri, R. A., Barnard, J. C., Chapman,  
587 E. G., ... Peckham, S. E. (2006, 11). Evolution of ozone, particulates, and  
588 aerosol direct radiative forcing in the vicinity of houston using a fully cou-  
589 pled meteorology-chemistry-aerosol model. *Journal of Geophysical Research*  
590 *Atmospheres*, 111. doi: 10.1029/2005JD006721
- 591 Feng, L., Smith, S. J., Braun, C., Crippa, M., Gidden, M. J., Hoesly, R., ... van der  
592 Werf, G. R. (2020, 2). The generation of gridded emissions data for cmip6.  
593 *Geoscientific Model Development*, 13, 461-482. doi: 10.5194/gmd-13-461-2020
- 594 Freitas, E. D., Rozoff, C. M., Cotton, W. R., & Dias, P. L. S. (2007, 1). Interac-  
595 tions of an urban heat island and sea-breeze circulations during winter over  
596 the metropolitan area of são paulo, brazil. *Boundary-Layer Meteorology*, 122,  
597 43-65. doi: 10.1007/s10546-006-9091-3
- 598 Gaubert, B., Bouarar, I., Doumbia, T., Liu, Y., Stavrakou, T., Deroubaix, A., ...  
599 Brasseur, G. P. (2021, 4). Global changes in secondary atmospheric pollu-

- 600 tants during the 2020 covid-19 pandemic. *Journal of Geophysical Research:*  
 601 *Atmospheres*, 126. doi: 10.1029/2020JD034213
- 602 Gettelman, A., Mills, M. J., Kinnison, D. E., Garcia, R. R., Smith, A. K., Marsh,  
 603 D. R., ... Randel, W. J. (2019, 12). The whole atmosphere community  
 604 climate model version 6 (waccm6). *Journal of Geophysical Research: Atmo-*  
 605 *spheres*, 124, 12380-12403. doi: 10.1029/2019JD030943
- 606 Giglio, L., Randerson, J. T., & van der Werf, G. R. (2013, 3). Analysis of daily,  
 607 monthly, and annual burned area using the fourth-generation global fire emis-  
 608 sions database (gfed4). *Journal of Geophysical Research: Biogeosciences*, 118,  
 609 317-328. doi: 10.1002/jgrg.20042
- 610 Granier, C., Darras, S., van der Gon, H. D., Doubalova, J., Elguindi, N., Galle, B.,  
 611 ... Sindelarova, K. (2019). The copernicus atmosphere monitoring service  
 612 global and regional emissions (april 2019 version). *Copernicus Atmosphere*  
 613 *Monitoring Service*. doi: 10.24380/d0bn-kx16
- 614 Grell, Peckham, S. E., Schmitz, R., McKeen, S. A., Frost, G., Skamarock, W. C.,  
 615 & Eder, B. (2005, 12). Fully coupled "online" chemistry within the  
 616 wrf model. *Atmospheric Environment*, 39, 6957-6975. doi: 10.1016/  
 617 j.atmosenv.2005.04.027
- 618 Guenther, a., Karl, T., Harley, P., Wiedinmyer, C., Palmer, P. I., & Geron, C.  
 619 (2006). Estimates of global terrestrial isoprene emissions using MEGAN  
 620 (Model of Emissions of Gases and Aerosols from Nature). *Atmospheric Chem-*  
 621 *istry and Physics Discussions*, 6, 107-173. doi: 10.5194/acpd-6-107-2006
- 622 Huang, G., Brook, R., Crippa, M., Janssens-Maenhout, G., Schieberle, C., Dore,  
 623 C., ... Friedrich, R. (2017, 6). Speciation of anthropogenic emissions  
 624 of non-methane volatile organic compounds: a global gridded data set for  
 625 1970-2012. *Atmospheric Chemistry and Physics*, 17, 7683-7701. doi:  
 626 10.5194/acp-17-7683-2017
- 627 Huneus, N., van der Gon, H. D., Castesana, P., Menares, C., Granier, C., Granier,  
 628 L., ... Ynoue, R. Y. (2020, 8). Evaluation of anthropogenic air pollutant  
 629 emission inventories for south america at national and city scale. *Atmospheric*  
 630 *Environment*, 235, 117606. doi: 10.1016/j.atmosenv.2020.117606
- 631 Ibarra-Espinosa, S., Ynoue, R. Y., Ropkins, K., Zhang, X., & de Freitas, E. D.  
 632 (2020, 2). High spatial and temporal resolution vehicular emissions in south-  
 633 east brazil with traffic data from real-time gps and travel demand models. *At-*  
 634 *mospheric Environment*, 222, 117136. doi: 10.1016/j.atmosenv.2019.117136
- 635 Inness, A., Aben, I., Ades, M., Borsdorff, T., Flemming, J., Jones, L., ... Ribas,  
 636 R. (2022, 11). Assimilation of s5p/tropomi carbon monoxide data with the  
 637 global cams near-real-time system. *Atmospheric Chemistry and Physics*, 22,  
 638 14355-14376. doi: 10.5194/acp-22-14355-2022
- 639 Inness, A., Ades, M., Agusti-Panareda, A., Barré, J., Benedictow, A., Blechschmidt,  
 640 A.-M., ... Suttie, M. (2019). The CAMS reanalysis of atmospheric com-  
 641 position. *Atmospheric Chemistry and Physics*, 19(6), 3515-3556. doi:  
 642 10.5194/acp-19-3515-2019
- 643 Kosmidis, E., Syropoulou, P., Tekes, S., Schneider, P., Spyromitros-Xioufis, E., Riga,  
 644 M., ... Alexandri, G. (2018, 5). hackair: Towards raising awareness about air  
 645 quality in europe by developing a collective online platform. *ISPRS Interna-*  
 646 *tional Journal of Geo-Information*, 7, 187. doi: 10.3390/ijgi7050187
- 647 Kumar, P., Morawska, L., Martani, C., Biskos, G., Neophytou, M., Sabatino,  
 648 S. D., ... Britter, R. (2015, 2). The rise of low-cost sensing for manag-  
 649 ing air pollution in cities. *Environment International*, 75, 199-205. doi:  
 650 10.1016/j.envint.2014.11.019
- 651 Levy, H. (1971, 7). Normal atmosphere: Large radical and formaldehyde concentra-  
 652 tions predicted. *Science*, 173, 141-143. doi: 10.1126/science.173.3992.141
- 653 Liang, J., Jackson, B., & Kaduwela, A. (2006, 9). Evaluation of the ability  
 654 of indicator species ratios to determine the sensitivity of ozone to reduc-

- 655 tions in emissions of volatile organic compounds and oxides of nitrogen  
 656 in northern california. *Atmospheric Environment*, *40*, 5156-5166. doi:  
 657 10.1016/j.atmosenv.2006.03.060
- 658 Liu, X., Ma, P.-L., Wang, H., Tilmes, S., Singh, B., Easter, R. C., ... Rasch,  
 659 P. J. (2016). Description and evaluation of a new four-mode version of  
 660 the modal aerosol module (mam4) within version 5.3 of the community at-  
 661 mosphere model. *Geoscientific Model Development*, *9*(2), 505-522. doi:  
 662 10.5194/gmd-9-505-2016
- 663 Mailler, S., Khvorostyanov, D., & Menut, L. (2013, 6). Impact of the vertical  
 664 emission profiles on background gas-phase pollution simulated from the emep  
 665 emissions over europe. *Atmospheric Chemistry and Physics*, *13*, 5987-5998.  
 666 doi: 10.5194/acp-13-5987-2013
- 667 Monks, P. S., Archibald, A. T., Colette, A., Cooper, O., Coyle, M., Derwent,  
 668 R., ... Williams, M. L. (2015, 8). Tropospheric ozone and its precur-  
 669 sors from the urban to the global scale from air quality to short-lived cli-  
 670 mate forcer. *Atmospheric Chemistry and Physics*, *15*, 8889-8973. doi:  
 671 10.5194/acp-15-8889-2015
- 672 NCEP. (2023). ds083.2, [dataset]. *US National Centers for Environmental Pre-*  
 673 *diction*. Retrieved from <https://10.5065/D6M043C6>, [Accessed:27/09/2023]  
 674 doi: 10.5065/D6M043C6
- 675 Nguyen, C. V., & Soulhac, L. (2021, 5). Data assimilation methods for urban air  
 676 quality at the local scale. *Atmospheric Environment*, *253*, 118366. doi: 10  
 677 .1016/j.atmosenv.2021.118366
- 678 OPENAQ. (2023). Openaq internet platform, [dataset]. *openaq.org*. Retrieved from  
 679 <https://openaq.org/>, [Accessed:04/11/2023]
- 680 Park, H.-S., Kim, R.-E., Park, Y.-M., Hwang, K.-C., Lee, S.-H., Kim, J.-J., ... Choi,  
 681 W. (2020, 2). The potential of commercial sensors for spatially dense short-  
 682 term air quality monitoring based on multiple short-term evaluations of 30  
 683 sensor nodes in urban areas in korea. *Aerosol and Air Quality Research*, *20*,  
 684 369-380. doi: 10.4209/aaqr.2019.03.0143
- 685 Petersen, A. K., Brasseur, G. P., Bouarar, I., Flemming, J., Gauss, M., Jiang, F., ...  
 686 Zhou, G. (2019, 4). Ensemble forecasts of air quality in eastern china-part 2:  
 687 Evaluation of the marcopolo-panda prediction system, version 1. *Geoscientific*  
 688 *Model Development*, *12*. doi: 10.5194/gmd-12-1241-2019
- 689 Pfister, G. G., Avise, J., Wiedinmyer, C., Edwards, D. P., Emmons, L. K., Diskin,  
 690 G. D., ... Wisthaler, A. (2011, 8). Co source contribution analysis for califor-  
 691 nia during arctas-carb. *Atmospheric Chemistry and Physics*, *11*, 7515-7532.  
 692 doi: 10.5194/acp-11-7515-2011
- 693 Powers, J. G., Klemp, J. B., Skamarock, W. C., Davis, C. A., Dudhia, J., Gill,  
 694 D. O., ... Duda, M. G. (2017). The weather research and forecasting model:  
 695 Overview, system efforts, and future directions. *Bulletin of the American*  
 696 *Meteorological Society*, *98*(8), 1717-1737. doi: 10.1175/BAMS-D-15-00308.1
- 697 Rémy, S., Kipling, Z., Flemming, J., Boucher, O., Nabat, P., Michou, M., ... Mor-  
 698 crette, J.-J. (2019, 11). Description and evaluation of the tropospheric aerosol  
 699 scheme in the european centre for medium-range weather forecasts (ecmwf)  
 700 integrated forecasting system (ifs-aer, cycle 45r1). *Geoscientific Model Develop-*  
 701 *ment*, *12*, 4627-4659. doi: 10.5194/gmd-12-4627-2019
- 702 Sokhi, R. S., Moussiopoulos, N., Baklanov, A., Bartzis, J., Coll, I., Finardi, S., ...  
 703 Kukkonen, J. (2022, 4). Advances in air quality research – current and emerg-  
 704 ing challenges. *Atmospheric Chemistry and Physics*, *22*, 4615-4703. doi:  
 705 10.5194/acp-22-4615-2022
- 706 Theloke, J., & Friedrich, R. (2007, 6). Compilation of a database on the composi-  
 707 tion of anthropogenic voc emissions for atmospheric modeling in europe. *Atmo-*  
 708 *spheric Environment*, *41*, 4148-4160. doi: 10.1016/j.atmosenv.2006.12.026
- 709 Venter, Z. S., Aunan, K., Chowdhury, S., & Lelieveld, J. (2020, 8). Covid-19 lock-

- 710 downs cause global air pollution declines. *Proceedings of the National Academy*  
711 *of Sciences*, *117*, 18984-18990. doi: 10.1073/pnas.2006853117
- 712 Viaene, P., Belis, C., Blond, N., Bouland, C., Juda-Rezler, K., Karvosenoja, N., ...  
713 Volta, M. (2016, 11). Air quality integrated assessment modelling in the con-  
714 text of eu policy: A way forward. *Environmental Science & Policy*, *65*, 22-28.  
715 doi: 10.1016/j.envsci.2016.05.024
- 716 Vivanco, M. G., & de Fatima Andrade, M. (2008). Relation between ozone levels  
717 and nox and voc emissions in the sao paulo metropolitan area for an episode of  
718 august, 1998. *International Journal of Environment and Pollution*, *35*, 90. doi:  
719 10.1504/IJEP.2008.021133
- 720 Wesseling, Ruiter, Blokhuis, Drukker, Weijers, Volten, ... Tielemans (2019, 8).  
721 Development and implementation of a platform for public information on air  
722 quality, sensor measurements, and citizen science. *Atmosphere*, *10*, 445. doi:  
723 10.3390/atmos10080445
- 724 Wiedinmyer, C., Akagi, S. K., Yokelson, R. J., Emmons, L. K., Al-Saadi, J. A., Or-  
725 lando, J. J., & Soja, A. J. (2011, 7). The fire inventory from ncar (finn): a  
726 high resolution global model to estimate the emissions from open burning.  
727 *Geoscientific Model Development*, *4*, 625-641. doi: 10.5194/gmd-4-625-2011
- 728 Zhang, Y., Wen, X., Wang, K., Vijayaraghavan, K., & Jacobson, M. Z. (2009, 11).  
729 Probing into regional o3 and particulate matter pollution in the united states:  
730 2. an examination of formation mechanisms through a process analysis tech-  
731 nique and sensitivity study. *Journal of Geophysical Research: Atmospheres*,  
732 *114*. doi: 10.1029/2009JD011900

733 **Appendix A Supplemental Tables and Figures (see separate document)**

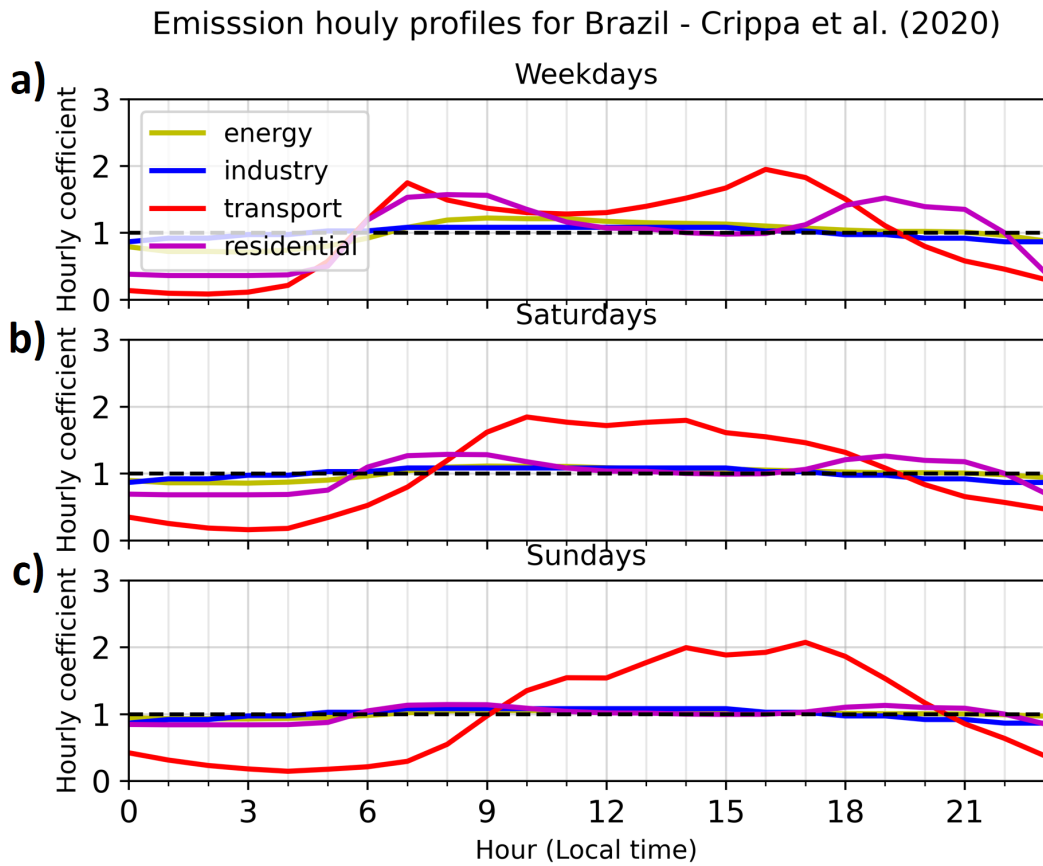


**Figure A1.** Sectoral hourly profiles of anthropogenic emission for Brazil proposed by Crippa et al. (2020).

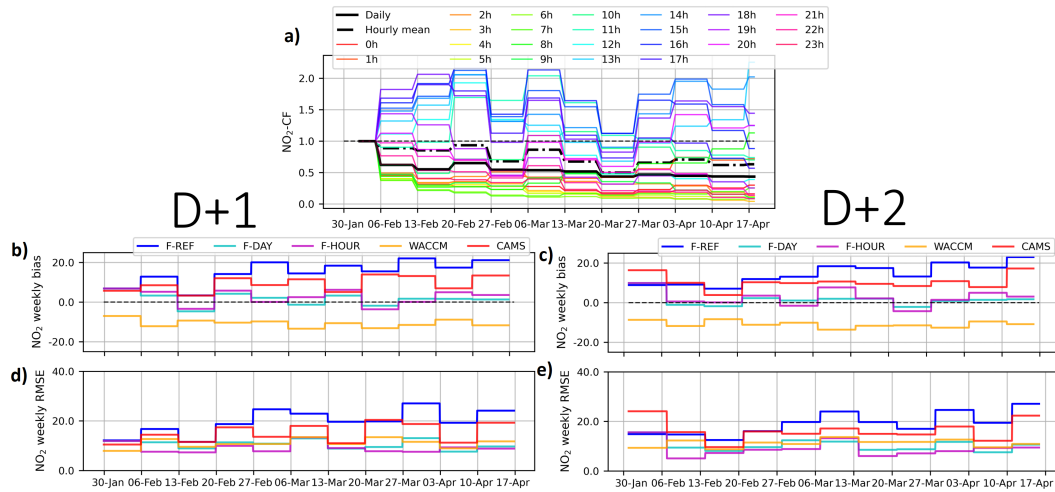


**Figure A2.** (a) Weekly evolution of daily and hourly  $\text{NO}_2$  correction factors (CF) used for the daily and hourly emission-scaled forecasts (F-DAY and F-HOUR) of a given week. Hours are given in local time (GMT-3). (b, c, d and e) Comparison of the weekly statistical performance (mean bias and RMSE) for  $\text{NO}_2$  concentration (in ppb) of the forecasts for the next day (d+1) and the day after (d+2) over the 10-week period (in 2023) in the center of São Paulo, for the three regional forecasts (F-REF, F-DAY and F-HOUR), and for the two global forecasts: (iv) WACCM provided by NCAR and (v) CAMS provided by ECMWF, over the 10-week period (in 2023) in the center of São Paulo.

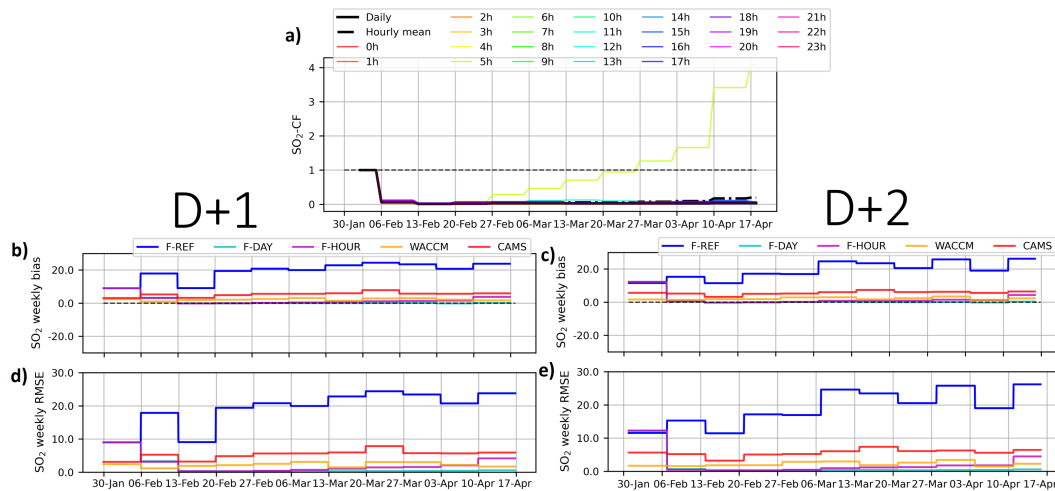


**Figure A3.** (a) Weekly evolution of daily and hourly  $\text{SO}_2$  correction factors (CF) used for the daily and hourly emission-scaled forecasts (F-DAY and F-HOUR) of a given week. Hours are given in local time (GMT-3). (b, c, d and e) Comparison of the weekly statistical performance (mean bias and RMSE) for  $\text{SO}_2$  concentration (in ppb) of the forecasts for the next day (d+1) and the day after (d+2) over the 10-week period (in 2023) in the center of São Paulo, for the three regional forecasts (F-REF, F-DAY and F-HOUR), and for the two global forecasts: (iv) WACCM provided by NCAR and (v) CAMS provided by ECMWF, over the 10-week period (in 2023) in the center of São Paulo.

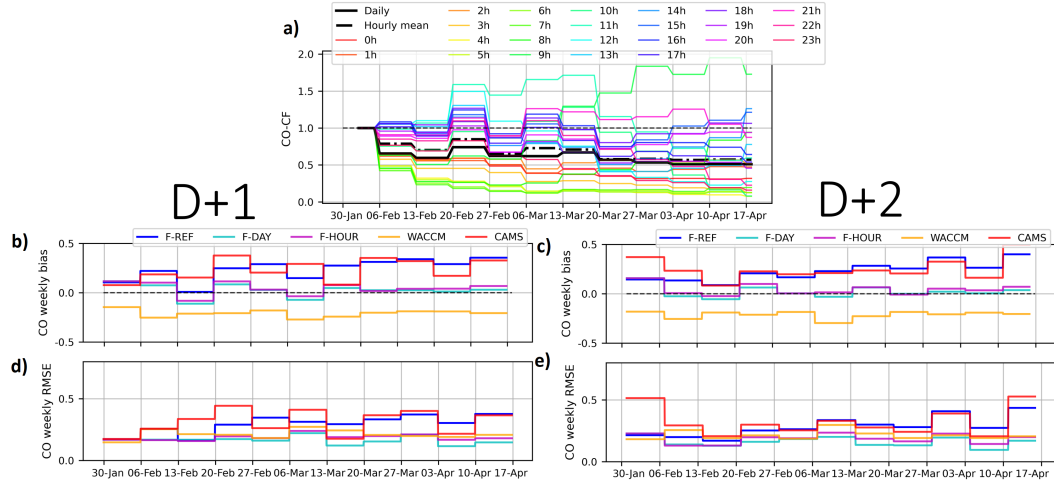


**Figure A4.** (a) Weekly evolution of daily and hourly CO correction factors (CF) used for the daily and hourly emission-scaled forecasts (F-DAY and F-HOUR) of a given week. Hours are given in local time (GMT-3). (b, c, d and e) Comparison of the weekly statistical performance (mean bias and RMSE) for CO concentration (in ppm) of the forecasts for the next day (d+1) and the day after (d+2) over the 10-week period (in 2023) in the center of São Paulo, for the three regional forecasts (F-REF, F-DAY and F-HOUR), and for the two global forecasts: (iv) WACCM provided by NCAR and (v) CAMS provided by ECMWF, over the 10-week period (in 2023) in the center of São Paulo.

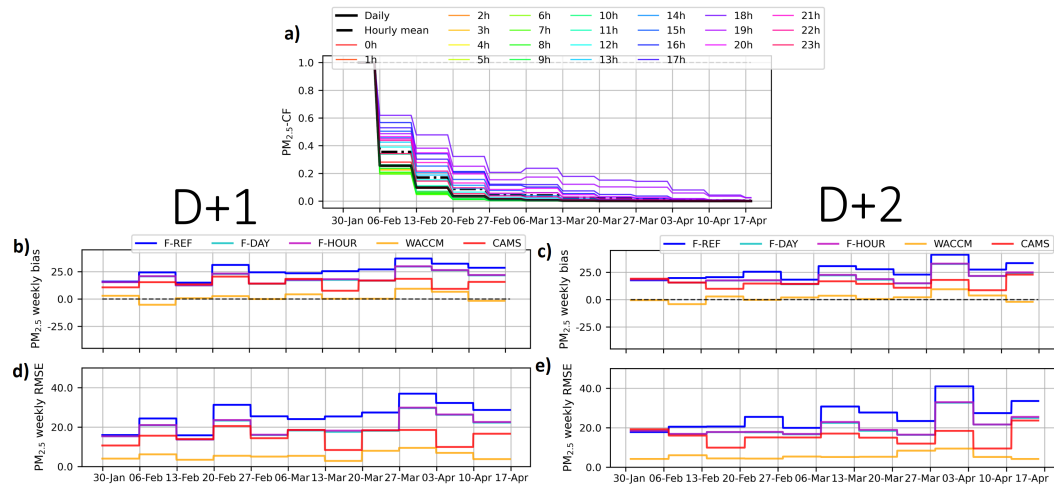


**Figure A5.** (a) Weekly evolution of daily and hourly PM<sub>2.5</sub> correction factors (CF) used for the daily and hourly emission-scaled forecasts (F-DAY and F-HOUR) of a given week. Hours are given in local time (GMT-3). (b, c, d and e) Comparison of the weekly statistical performance (mean bias and RMSE) for PM<sub>2.5</sub> concentration (in  $\mu\text{g}\cdot\text{m}^{-3}$ ) of the forecasts for the next day (d+1) and the day after (d+2) over the 10-week period (in 2023) in the center of São Paulo, for the three regional forecasts (F-REF, F-DAY and F-HOUR), and for the two global forecasts: (iv) WACCM provided by NCAR and (v) CAMS provided by ECMWF, over the 10-week period (in 2023) in the center of São Paulo.

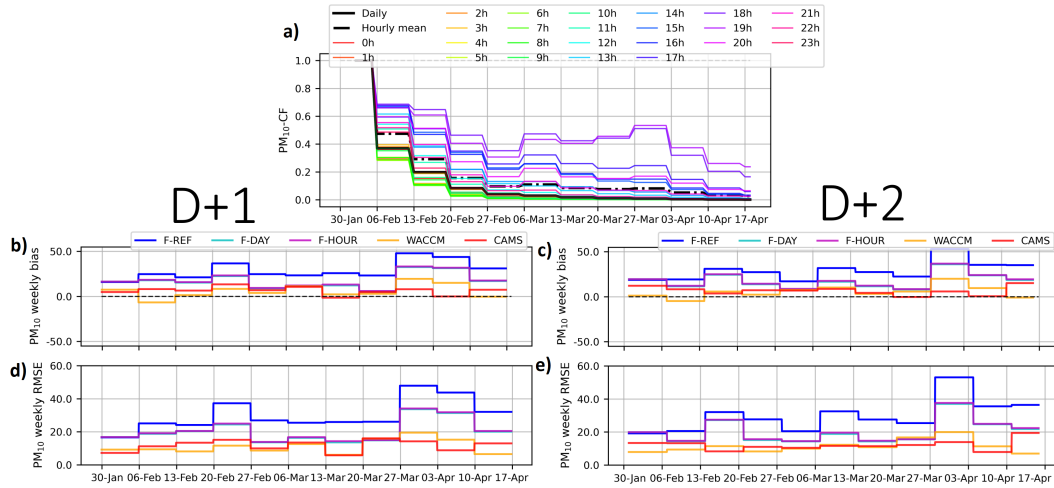


**Figure A6.** (a) Weekly evolution of daily and hourly  $PM_{10}$  correction factors (CF) used for the daily and hourly emission-scaled forecasts (F-DAY and F-HOUR) of a given week. Hours are given in local time (GMT-3). (b, c, d and e) Comparison of the weekly statistical performance (mean bias and RMSE) for  $PM_{10}$  concentration (in  $\mu g \cdot m^{-3}$ ) of the forecasts for the next day (d+1) and the day after (d+2) over the 10-week period (in 2023) in the center of São Paulo, for the three regional forecasts (F-REF, F-DAY and F-HOUR), and for the two global forecasts: (iv) WACCM provided by NCAR and (v) CAMS provided by ECMWF, over the 10-week period (in 2023) in the center of São Paulo.

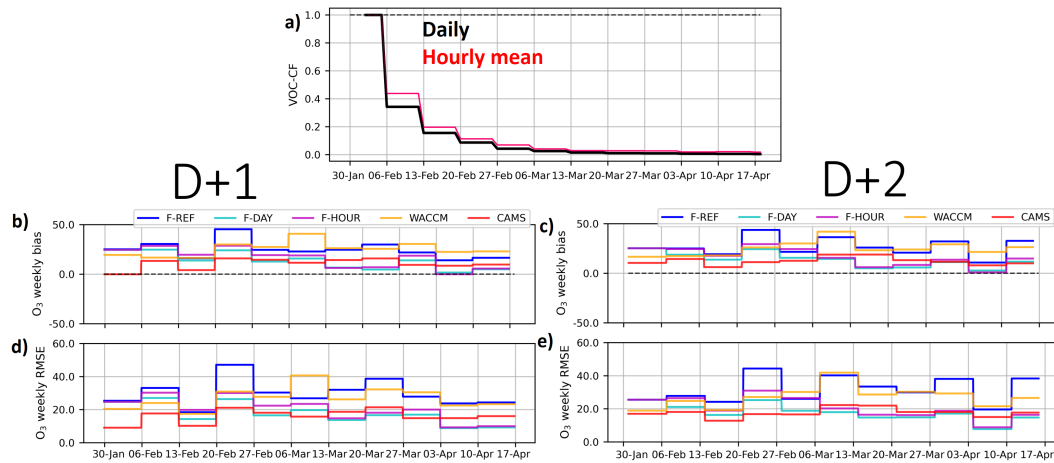


**Figure A7.** (a) Weekly evolution of daily and hourly  $O_3$  correction factors (CF) used for the daily and hourly emission-scaled forecasts (F-DAY and F-HOUR) of a given week. Hours are given in local time (GMT-3). (b, c, d and e) Comparison of the weekly statistical performance (mean bias and RMSE) for  $NO_2$  of the forecasts for the next day (d+1) and the day after (d+2) over the 10-week period (in 2023) in the center of São Paulo, for the three regional forecasts (F-REF, F-DAY and F-HOUR), and for the two global forecasts: (iv) WACCM provided by NCAR and (v) CAMS provided by ECMWF, over the 10-week period (in 2023) in the center of São Paulo.

**Table A1.** Configurations of the air quality models for which the forecasts are analyzed: the WACCM forecast (provided by NCAR), the CAMS forecast (provided by ECMWF) and the regional forecasts made with the WRFchem model.

<b>Forecast Institution Model</b>	WACCM NCAR CESM2	CAMS ECMWF IFS	F-REF, F-DAY, F-HOUR MPI-IUP WRFchem (version 4.3.3)
<i>Domain</i>			
<b>Horizontal resolution</b>	0.95° × 1.25°	40 km	10 km
<b>Domain extension</b>	Global	Global	regional (80 x 80 grid cells)
<b>Vertical levels</b>	70	137	37
<b>Output frequency</b>	6h	3h	1h
<i>Emission</i>			
<b>Anthropogenic</b>	CMIP6 (Feng et al., 2020)	CAMS-GLOB-ANTv5.3 (Granier et al., 2019)	CAMS-GLOB-ANTv4.2 (Granier et al., 2019)
<b>Anthr. temporal profiles</b>	None	CAMS-GLOB-ANTv5.3	(Crippa et al., 2020)
<b>Anthr. vertical profiles</b>	None	CAMS-GLOB-ANTv5.3	(Mailler et al., 2013)
<b>Biogenic</b>	MEGANv2.1 (Guenther et al., 2006)	MEGANv2.1 (Guenther et al., 2006)	MEGANv2.1 (Guenther et al., 2006)
<b>Fires</b>	GFED4 (Giglio et al., 2013)	CAMS-GFASv1.4 (Inness et al., 2022)	FINNv1 (NRT) (Wiedinmyer et al., 2011)
<i>Gas and aerosol</i>			
<b>Chemical mechanism</b>	MOZART4-T1 (Emmons et al., 2020)	CB05 (Inness et al., 2019)	MOZART4 (Emmons et al., 2010)
<b>Aerosol scheme</b>	MAM4 (Liu et al., 2016)	IFS-AER (Rémy et al., 2019)	GOCART (Chin et al., 2002)
<b>Boundary conditions</b>	None	None	WACCM